Hindawi
Journal of Oncology
Volume 2019, Article ID 9685476, 12 pages
https://doi.org/10.1155/2019/9685476

Review Article

Role of Simulations in the Treatment Planning of Radiofrequency Hyperthermia Therapy in Clinics

Bibin Prasad[1,2] **Jung Kyung Kim**[3] **and Suzy Kim**[1]

[1]*Department of Radiation Oncology, SMG-Seoul National University Boramae Medical Center, Seoul 07061, Republic of Korea*
[2]*Department of Radiology, UT Southwestern Medical Center, Dallas, TX 75390-8542, USA*
[3]*School of Mechanical Engineering and Department of Integrative Biomedical Science and Engineering, Graduate School, Kookmin University, Seoul 02707, Republic of Korea*

Correspondence should be addressed to Jung Kyung Kim; jkkim@kookmin.ac.kr and Suzy Kim; suzy101@snu.ac.kr

Received 13 June 2019; Revised 20 July 2019; Accepted 28 July 2019; Published 29 August 2019

Academic Editor: San-Lin You

Hyperthermia therapy is a treatment modality in which tumor temperatures are elevated to higher temperatures to cause damage to cancerous tissues. Numerical simulations are integral in the development of hyperthermia treatment systems and in clinical treatment planning. In this study, simulations in radiofrequency hyperthermia therapy are reviewed in terms of their technical development and clinical aspects for effective clinical use. This review offers an overview of mathematical models and the importance of tissue properties; locoregional mild hyperthermia therapy, including phantom and realistic human anatomy models; phase array systems; tissue damage; thermal dose analysis; and thermoradiotherapy planning. This review details the improvements in numerical approaches in treatment planning and their application for effective clinical use. Furthermore, the modeling of thermoradiotherapy planning, which can be integrated with radiotherapy to provide combined hyperthermia and radiotherapy treatment planning strategies, are also discussed. This review may contribute to the effective development of thermoradiotherapy planning in clinics.

1. Introduction

Hyperthermia therapy is used as an adjunctive cancer treatment modality in which the temperature of cancerous tissues is increased to enhance the clinical efficacy of chemotherapy and radiotherapy [1–4]. Radiofrequency (RF) generator with electrode/antenna is a technique through which hyperthermia therapy can be achieved. RF (100 kHz–3 GHz) is a form of electromagnetic (EM) energy that comprises an alternating electric current, and this EM energy is absorbed when passing through the human body to target tumor tissues as tumors have different dielectric properties compared with those of surrounding normal tissues [5]. During hyperthermia treatment, the tumor temperature is increased to 40°C–45°C for 30–60 min for effective radio and chemosensitization and the blood perfusion is increased [6, 7].

Hyperthermia treatment planning (HTP) includes the selection of an optimal treatment technique that is in current use and for which several tools and techniques have been developed. Previous review articles have shown that HTP is an essential approach and has a pivotal role in the control, improvement, and assessment of hyperthermia treatment quality [6–8]. HTP, which involves obtaining patient data and calculating power deposition and temperature distribution in tissues, enables improvements in treatment quality [8]. To provide a complete 3D distribution of temperature in the human body, treatment planning must consider complex heating systems, human anatomy, dielectric tissue properties, thermophysical changes in tissues in response to heat and physiology, especially blood perfusion [9]. For clinical applications, high-resolution patient imaging, specific absorption rate (SAR) and thermal models, evaluation software, and data acquisition systems are available these days [7].

To improve treatment quality, simulation techniques have been extensively used in clinics, and HTP techniques have been developed for clinical use [10–13]. An HTP system called HyperPlan was assessed for its clinical practicability in predicting the toxicity and efficacy of hyperthermia treatment [14]. VEDO (visualization tool for electromagnetic dosimetry and optimization) is an HTP software tool developed for quantitative optimization of SAR in clinical head and neck cancer treatment [11]. Clinical trials have been conducted to verify HTP calculations by measuring the SAR in 11 patients with uterine cervical cancer using the 70-MHz Academic Medical Center (AMC)-4 waveguide system [15]. Another clinical trial assessed the feasibility of HGS (online HTP-guided steering) in improving the treatment quality for locally advanced cervical cancer [10].

Commercial software packages are available for HTP. The most widely used simulation software for locoregional hyperthermia treatment is Sigma HyperPlan (Dr. Sennewald Medizintechnik GmbH, Munchen, Germany), which was developed by the Konrad Zuse Institute; however, this software is limited to modeling locoregional hyperthermia systems. More flexible treatment planning systems have been developed, including the AMC DIVA HTP system (AMC, Amsterdam, Netherlands), SEMCAD X (SPAEG, Zurich, Switzerland), and Sim4Life (ZMT, Zurich, Switzerland), which include additional and advanced treatment planning tools such as animal and human phantom models, tissue models, magnetic resonance imaging (MRI) modules, and dispersive fitting modules. Besides these specialized HTP tools, general commercial software, including COMSOL Multiphysics (http://www.comsol.com), CST Studio Suite (http://www.cst.com), and Ansys (http://www.ansys.com), can also be used for calculating EM and temperature distributions. Figure 1 presents the 3D modeling, SAR distribution, temperature distribution, and thermal dose calculations in a patient-specific human model simulated with Sim4Life software [5].

This review summarizes the various technical aspects in radiofrequency hyperthermia, including mathematical models, tissue properties, phantom studies, realistic human anatomy, tissue damage and thermal dose, and thermoradiotherapy planning.

2. Numerical Modeling

A summary of the major mathematical models used for HTP is detailed below. The EM field distribution during RF heating can be calculated using Maxwell's equation. The finite-difference time-domain (FDTD) method can be used for a wide range of frequencies (250 Hz–3 GHz) [9, 16–25]:

$$\varepsilon \frac{\delta E}{\delta t} + J = \nabla H - \frac{\delta B}{\delta t} = \nabla E, \tag{1}$$

$$\frac{\partial E_z}{\partial t} = \frac{1}{\varepsilon}\left(\frac{\partial H_y}{\partial x} - \frac{\partial H_x}{\partial y} - \sigma E_z\right), \tag{2}$$

where ε is the relative permittivity, E is the electric field strength ($\mathrm{V{\cdot}m^{-1}}$), J is the current density ($\mathrm{A{\cdot}m^{-2}}$), H is the magnetic field strength ($\mathrm{A{\cdot}m^{-1}}$), B is the magnetic flux density (T), and σ is the electrical conductivity ($\mathrm{S{\cdot}m^{-1}}$).

The vector equations in equation (1) are written as six separate partial differential equations, one of which is shown as equation (2) [25].

For capacitive heating, quasistatic approximation is used to obtain the potential distribution [26–29]:

$$\begin{aligned} \nabla(-\varepsilon\nabla\phi) &= 0, \\ E &= -\nabla\phi, \end{aligned} \tag{3}$$

where ϕ is the electric potential (V).

The E-field calculation from the FDTD and quasistatic approaches enables the calculation of the SAR in tissues [29]:

$$\begin{aligned} \mathrm{SAR} &= \frac{\sigma}{2\rho}|E|^2, \\ Q_r &= \rho\mathrm{SAR} = \frac{\sigma}{2}|E|^2, \end{aligned} \tag{4}$$

where ρ is the mass density ($\mathrm{kg{\cdot}m^{-3}}$), SAR is the specific absorption rate ($\mathrm{W{\cdot}kg^{-1}}$), and Q_r is the EM power absorbed ($\mathrm{W{\cdot}m^{-3}}$).

The RF energy obtained from the EM simulation is given as a heat source (Q_r) to the Pennes bioheat model to calculate the temperature distribution [30–32]:

$$\rho c \frac{\partial T}{\partial t} = \nabla \cdot (k\nabla T) - \omega_b c_b (T - T_b) + Q_r + Q_m, \tag{5}$$

where c is the specific heat ($\mathrm{J{\cdot}kg^{-1}{\cdot}K^{-1}}$); T is the temperature (K); t is the time (s); k is the thermal conductivity ($\mathrm{W{\cdot}m^{-1}{\cdot}K^{-1}}$); Q_m is the metabolic heat generation rate ($\mathrm{W{\cdot}m^3}$); ω_b is the blood perfusion rate ($\mathrm{kg{\cdot}m^{-3}{\cdot}s^{-1}}$); and c_b and T_b correspond to the specific heat and temperature of blood, respectively.

Besides the temperature distribution, thermal dose can be obtained using the cumulative equivalent minutes (CEM at 43°C) [33]:

$$\mathrm{CEM43} = \int_{t_0}^{t_{\mathrm{final}}} R^{43-T(t)} dt, \tag{6}$$

where R is the temperature dependence of the rate of cell death ($R = 0.5$ for $T > 43^\circ\mathrm{C}$, $R = 0.25$ for $39^\circ\mathrm{C} \geq T \geq 43^\circ\mathrm{C}$, and $R = 0$ for $T < 39^\circ\mathrm{C}$), dt is the time interval with which temperature measurements are made (min), and t_o (min) and t_{final} (min) are the initial and final heating periods, respectively.

The combined therapeutic outcomes of radiotherapy and hyperthermia can be calculated in terms of the equivalent radiation dose as follows [34]:

$$\mathrm{EQD}_{RT} = \frac{\alpha(T)D + G\beta D^2}{\alpha + \beta d}, \tag{7}$$

where α ($\mathrm{Gy^{-1}}$) and β ($\mathrm{Gy^{-2}}$) are the radiosensitivity parameters at 37°C, $\alpha(T)$ is the temperature-dependency of α, d is the fractionated dose (Gy), D is the total radiation dose (Gy), and G is the Lea–Catcheside protraction factor.

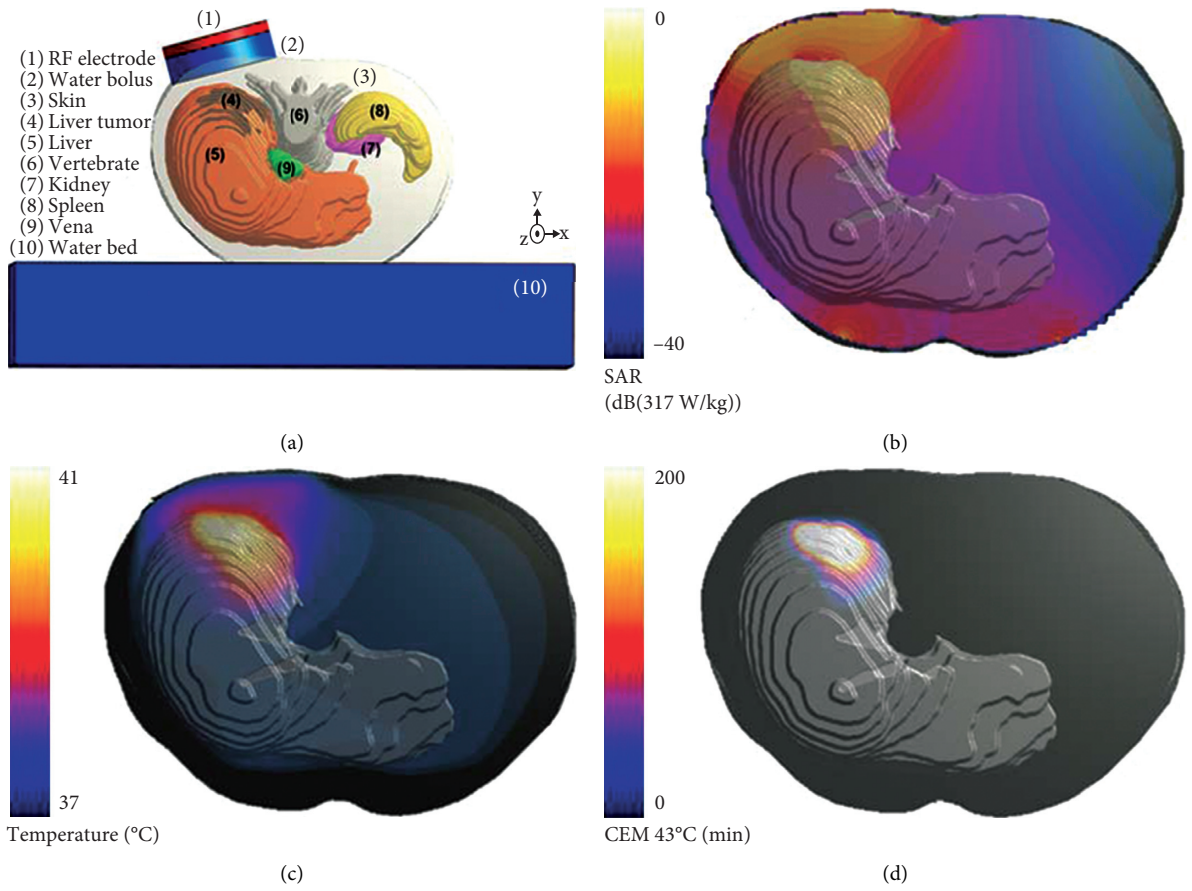

Figure 1: Computational modeling and analysis using a patient-specific liver tumor model: (a) 3D human anatomy with an RF system; (b) SAR distribution; (c) temperature distribution; (d) thermal dose.

3. Tissue Properties

Tissue properties are important parameters in simulations in determining the temperature distribution of the target and its surrounding tissues. Electrical conductivity, relative permittivity, density, thermal conductivity, specific heat, metabolic heat generation rate, and blood perfusion rate are the major tissue properties associated with the electrothermal simulations of mild and ablative hyperthermia [35]. Several studies have been conducted for the measurement of normal tissue properties, and a wide database is available [36–39]. The most complete database for tissue properties is available at IT'IS Foundation (itis.swiss/database) [40]. In RF thermal therapy, the dielectric properties (electrical conductivity and relative permittivity) are the most important properties in calculating energy deposition in tissues. Previous studies have reported that the dielectric properties of tissues vary as the frequency increases [36–38]. Tumors present a very wide distribution of electrical properties [41]. Generally, tumor tissues exhibit a high dielectric property compared with that exhibited by normal tissues; however, certain tumors exhibit low dielectric properties compared with that exhibited by normal tissues [39, 42–44]. Studies have also reported that there are variations in tumor properties in different patients and different cancer stages and that these effects required further evaluations [45, 46]. A simulation study showed that calculations with different dielectric properties lead to different SAR, temperatures, and thermal dose calculations [29]. Tables 1 and 2 summarize the various tumor phantom/tissue properties considered in simulation studies at different frequencies.

Some of the properties displayed in Tables 1 and 2 may be based on certain assumptions such as high/low electrical conductivity, relative permittivity, and blood perfusion. However, certain tumor property measurements have been reported based on human tumor samples, [39, 45, 46, 59, 60], which will be more correct to use in simulations, thereby providing more accurate SAR/temperature distributions. The temperature-dependency of electrical and thermal properties must be considered important for hyperthermia and ablative temperature treatment planning to enhance the accuracy of treatments [35, 61, 62]. In the case of thermal conductivity, the change correlates directly with temperature, whereas for blood perfusion, a strong irreversible component is observed with the interaction with time and temperature. There will be an increase in blood perfusion at mild hyperthermia temperatures and collapse in blood flow at ablative temperatures. For dielectric properties at RF frequencies, the tissue state, such as in vivo, in situ, and ex

Table 1: Dielectric and thermal properties of tumor phantom used in simulations at different frequencies from the literature.

Frequency (MHz)	Tumor phantom type	Density ($kg \cdot m^{-3}$)	Relative permittivity	Electrical conductivity ($S \cdot m^{-1}$)	Specific heat ($J \cdot kg^{-1} \cdot K^{-1}$)	Thermal conductivity ($W \cdot m^{-1} \cdot K^{-1}$)	Reference
13.56	Egg white	1131	66	0.705	2679	0.393	Hossain et al. [47]
26	Agarose	1020	79.86	0.6	4267	0.555	Kim et al. [49]
36	Agarose	1020	80	1.38	4267	0.555	Kim et al. [50]
110	Agar	900	80	0.70	3500	0.210	Kowalski and Jin [51]
165	Agar	1021	74.15	2.97	4200	0.498	Oh et al. [52]

Table 2: Dielectric and thermal properties of different cancer used in simulations at different frequencies from the literature.

Frequency (MHz)	Cancer type	Density ($kg \cdot m^{-3}$)	Relative permittivity	Electrical conductivity ($S \cdot m^{-1}$)	Specific heat ($J \cdot kg^{-1} \cdot K^{-1}$)	Thermal conductivity ($W \cdot m^{-1} \cdot K^{-1}$)	Blood perfusion ($kg \cdot m^{-3} \cdot s^{-1}$)	Reference
13.56	Liver	1078.75	70	0.5	3763	0.5191	2.15	Prasad et al. [5]
13.56	Muscle	1070	278.85	0.7847	3421.2	0.4949	0.35	Prasad et al. [29]
70	Cervical, pancreas, Esophagus, Prostate	1050	65	0.74	3639	0.56	1.8	Kok et al. [13, 26, 53, 54], Crezee et al. [55]
100	Cervical	1050	58	0.78	3639	0.56	1.8	Kok et al. [13]
120	Cervical	1050	55	0.80	3639	0.56	1.8	Kok et al. [13]
130	Cervical	1050	54	0.81	3639	0.56	1.8	Kok et al. [13]
140	Cervical	1050	53	0.82	3639	0.56	1.8	Kok et al. [13]
150	Cervical	1050	52	0.83	3639	0.56	1.8	Kok et al. [13]
434	Head and neck	1050	59.0	0.89	3950	0.51	7.35, 1.32*/ 15.58*	Verhaart et al. [56], Paulides et al. [57], Drizdal et al. [58]*

vivo, with time after tissue extraction has a significant impact on dielectric property measurement, which needs to be considered [35].

4. Locoregional Hyperthermia Therapy

Locoregional therapy is usually applied at hyperthermic temperature of 40°C–45°C. Studies with tissue-mimicking phantom models and 3D human anatomy models have been conducted to demonstrate its efficacy in the treatment of various types of cancer as summarized below.

4.1. Tissue-Mimicking Phantom Models. Tissue-mimicking phantoms, the physical properties of which are close to human tissues, are important in the development of experimental and numerical techniques. Many studies have been performed to develop phantoms with dielectric and thermal properties similar to those of human tissues [63–74]. An agar phantom that is suitable for use in simulations was developed in the 5–40 MHz range. This type of phantom has distinct advantages, including the ability to vary its dielectric properties, retain its original shape, and avoid deorientation by molding for one year [63]. Cylindrical phantoms are commonly used to investigate various RF hyperthermia mechanisms, and selective and deep heating characteristics have been evaluated with cylindrical phantoms experimentally and numerically for 13.56 MHz RF hyperthermia systems [47]. Simulations and experiments have been performed using a cylindrical phantom with fat and muscle layers to determine the effect of large vessel counterflow on temperature distribution by hyperthermia [75]. A computational phantom comprising fat, muscle, and tumor tissues has been used for temperature prediction validation in the development of a temperature-based feedback control system for an EM-phased array hyperthermia system [51]. Simulations on a cylindrical split phantom have also comprised vegetable oil and saline with dielectric properties similar to those of human tissues for B_{1+} imaging to validate SAR models for RF hyperthermia [76]. SAR distribution for centrally located targets in tissue-equivalent phantoms has been simulated, with optimal distributions established at 140 MHz [13]. The size of SAR hot spots was reduced at higher frequencies when simulations were performed in the range of 64–600 MHz [77]. Temperature increase due to SAR from RF fields has been numerically and experimentally validated with phantom models that provide good agreement and demonstrate the possibility of using simulations to ensure safety during MRI [52]. The feasibility of using nanoparticles with RF systems has been reported with phantom models to increase tissue temperature in localized and deep-seated tumor regions [49, 50, 77]. The addition of magnetic nanoparticles to regions drew more heat than that by surrounding regions in

both simulations and MR thermometry [50], and a two-channel RF system exhibited superior capability in localizing heat to the nanoparticle-mediated tumor region compared with that in the normal region [77].

4.2. Realistic Human Anatomy Models. The accurate prediction of SAR and temperature distribution in human tissues is necessary for the effective use of RF-induced hyperthermia in clinics. By using patient-specific computational models, HTP quality can be improved. Numerical simulations with phantom and human anatomy models can evaluate the efficacy of RF techniques developed for clinical use. A 3D model derived from human anatomical data showed that simulations can assist in the clinical use of RF applicators to heat the region of the thorax [78]. In patients with malignant brain tumors, computer simulations showed good agreement with measurements for interstitial hyperthermia [79, 80]. Temperature measurement and simulations in 11 human subjects with intracranial tumors showed a difference of approximately ±0.75°C [79], and a difference of only 0.4°C was obtained in 4 patients with malignant glioma [80]. The RF EM field patterns obtained from simulations in human anatomies was verified using the MR B_{1+} imaging technique with an accuracy of 3.5%, suggesting that the MR B_{1+} imaging technique is a valuable technique for obtaining the dielectric interaction between human anatomy and the RF field [81]. MR B_{1+} is an experimentally validated technique for hyperthermia SAR treatment planning [76]. Given that SAR is a major parameter in MRI safety regulation [82], patient-specific local SAR determination with MRI measurements and simulation yields accurate estimation of SAR for the brain [82]. The efficacy of RF hyperthermia therapy can be further improved by incorporating MR B_{1+} imaging and SAR determination technique [81, 82] with necessary modifications in HTP. Minimally invasive 3D dosimetry based on patient-specific simulations and sensory feedback was found to be feasible for use in hyperthermia therapy. The prediction of the T50 treatment parameter had a median accuracy of 0.4°C with patient-specific properties [56]. Patient-specific simulations in the treatment of liver cancer showed its capability to heat tumors with 13.56 MHz RF hyperthermia selectively and demonstrated the effect of electrode size and power modulation in predicting temperature distribution and thermal dose for effective clinical treatment planning [5].

Among RF hyperthermia systems, RF phased array applicators are effectively used in clinics for the selective heating of tumor tissues while sparing normal healthy tissues [83]. There have been several developments in system design to improve its efficacy in clinical use. A considerable improvement in the focusing of SAR distribution in tumor regions was observed when parameters, such as frequency (100–120 MHz), bolus chamber (tapered), dipole length (17–30 cm), and phase and amplitude of power to various dipoles, were adjusted in numerical calculation using an annular phase array of eight dipole antennas coupled with water bolus on human anatomy [84]. Furthermore, when the previous validation of RF hyperthermia array modeling with EM field distribution measurement considered variations in bolus size and waveguide quantity, the accuracy was found to be inadequate for quantitative SAR dosimetry for individual patients [85]. The technological development of RF phased array hyperthermia has been achieved by developing a treatment planning program. Improvements in the index temperature of 1°C–2°C were achieved when the single ring was upgraded to a triple ring with free-phase selection for individual antenna or as pairs [86]. Temperature-based optimization for HTP with high resolution was implemented to maximize tumor temperature using E-field distributions as a primary input. The method was found to work well in clinical situations [53]. A prospective HTP together with high-resolution temperature optimization improved the treatment in 16 patients with esophageal cancer [87]. A useful tool for optimizing clinical treatments was provided by advancing the simulation accuracy with temperature-dependent blood perfusion and noninvasive thermometry with thermal imaging. The quality of hyperthermia treatment can be improved by performing simulations routinely as part of pretreatment planning in clinics [88]. For the planning, evaluation, and optimization of hyperthermia treatments, the flexible software package Plan2Heat was developed. Plan2Heat performs EM and temperature simulations for RF and other treatment techniques. The package also enables the sophisticated thermal modeling of 3D vasculature using a vessel generation algorithm. The source code of the software allows the easy extension of the software package for future applications [26].

A potential hyperthermia-phased array treatment system for head and neck cancer has been investigated and developed successfully with the assistance of numerical simulations that consider various parameters [89], and an efficient treatment system HYPERcollar was developed with an antenna ring, water bolus, and a positioning system [57]. Numerical simulations enhanced the stability, water bolus shape, skin contact, and positioning of patients (±5 mm), improving patient treatment quality, reproducibility, operator handling, and patient safety [90]. In a study of 27 patients, pretreatment planning involved the use of 3D human models to determine the SAR target level of 25% and to decide whether hyperthermia treatment was possible in patients. The study confirmed the feasibility and safety of hyperthermia therapy with promising outcomes and good compliance [91]. To further investigate the treatment quality of HYPERcollar, comparisons were made with planar applicators, including the lucite cone applicator (LCA) and current sheet applicator (CSA), in 24 patients with a clinical target volume of up to 6 cm from the surface. Simulations revealed that HYPERcollar was the preferred system over the LCA and CSA [58].

Water bolus temperature influences the prediction of tissue temperature in hyperthermia therapy. 3D EM and thermal simulations were performed to develop a guideline for water bolus temperature for the LCA [92]. A convective coefficient for the skin and water bolus surface was used, and convective coefficients of different water boluses were

measured (75–125 $W \cdot m^{-2} \cdot K^{-1}$). The 3D model consisting LCA, water bolus, and a block of tissue was evaluated by comparing simulations with clinical measurements, and the temperature distribution of tissues was predicted well on a global view, but some temperature probes showed a deviation of 1.5°C–2.0°C [92]. Water bolus temperature was also assumed to be constant in hyperthermia simulations. In a patient-specific simulation of liver cancer treatment with RF hyperthermia, the water bolus temperature was kept constant at 25°C to keep the surface cool to prevent skin burning [5]. Moreover, in capacitive hyperthermia treatment for lung cancer using a human thorax model, the water bolus surrounding the thorax region is maintained at a constant temperature [93]. In HYPERcollar systems for head and neck hyperthermia, the water bolus shape has a significant impact. With high reproducibility, water bolus can reduce the risk of underexposure and nearly the whole head and neck of the patient can be enclosed with surrounding water bolus, improving the treatment quality [58, 90, 94].

5. Estimation of Thermal Tissue Damage

The thermal dose (cumulative equivalent minutes at 43°C, CEM43) model is mainly used to calculate tissue damage during hyperthermia therapy [33]. Thermal thresholds for tissue damage have been investigated, and preclinical and clinical examinations have been conducted to assess the tissue damage in various types of tissues [95–103]. By using optimized time-dependent temperature distribution in tumor tissues, tissue damage can be preplanned to predict clinical outcomes [29]. The effect of thermal wave characteristics on thermal dose distribution was numerically evaluated during thermal therapy. For total deposited energy, the time lag of the peak temperature became pronounced, and the peak level was decreased with increasing relaxation time. No significant difference was observed in thermal dose distribution with or without the effect of thermal relaxation time [104]. To determine the safety of RF-induced local thermal hot spots using a 1.5-T body coil, simulations were performed on four anatomical models of varying sizes and shapes, and the results suggested that a thermal dose is recommended rather than SAR or temperatures to ensure safety [105]. SAR thresholds were quantified for electromagnetic exposure using functional thermal dose limits. From the literature, the lowest thermal dose required to induce acute local tissue damage was used to calculate the corresponding thermal dose functional SAR limits. The results were evaluated by comparing the calculations of a real human anatomy simulation for head and neck hyperthermia treatment. It was found that for muscle tissues, the current restriction on 10 g peak spatial average SAR can reach up to 31.2 W/kg. Therefore, they suggested exposure-specific guidelines (i.e., exposure-specific SAR limits) rather than the current generic guidelines for safety [106]. Thermal dose calculations in a patient-specific simulation study for liver cancer treatment also predicted that no damage occurs at normal tissues while selectively increasing the tumor temperature, indicating that it is a promising technique for HTP [5]. In HTP, tumor property variations may also require consideration for precise tissue damage calculations. When thermal dose simulations were compared with dielectric properties measured versus dielectric properties obtained from a previous study using a mouse tumor model, accurate thermal dose calculations were obtained when the measured dielectric properties of the tumor were used in simulations [29].

6. Thermoradiotherapy Planning

Substantial prospective and randomized clinical data show the clear benefits of combined hyperthermia and radiotherapy for various types of cancer [107]. A method for estimating the therapeutic effect of radiation and hyperthermia can be numerically quantified in terms of equivalent radiation dose. The temperature-dependent parameters α and β of the linear-quadratic (LQ) model can effectively express radiosensitization by hyperthermia [54]. The LQ parameters of human tumors can be useful for the prediction of radiobiological response in clinical radiotherapy [108]; however, few studies have reported the LQ parameters at hyperthermic temperatures [109, 110]. Numerical models were developed to calculate equivalent radiation dose and analysis for patients with prostate and cervical cancers, and these models revealed an escalation in equivalent radiation dose [54, 55]. For the planned average minimum, mean, and maximum tumor temperatures (40.5°C, 41.6°C, and 42.4°C, respectively) and the radiation therapy doses of 62.9, 76, and 81 Gy, respectively, the equivalent radiation doses increased to 70.3, 86.3, and 93.6 Gy, respectively, with an extended isodose level of 95% [54] in patients with prostate cancer. Biological modeling to quantify radiosensitization in patients with cervical cancer in terms of equivalent dose for combined radiotherapy and hyperthermia resulted in an increase in the radiation dose from 7.3 to 11.9 Gy compared with that for radiotherapy alone [55]. Equivalent radiation dose calculation with RF hyperthermia for human lung cancer xenografts using A549 and NCI-H1299 cell lines showed that a higher radiation dose escalation was observed for NCI-H1299 compared with that observed for A549 (36.07 Gy for A549 cells and 39.66 Gy for NCI-H1299 cells from 20 Gy) [111].

The X-Term software package was developed to calculate the equivalent radiation dose using an extended version of the LQ model. The software can support decision-making for optimal clinical treatment, enabling the biological evaluation of thermoradiotherapy plans via equivalent 3D radiation dose distributions [34]. It is important that planning combines both radiation and hyperthermia therapy by considering the synergistic actions of the two modalities. The first planning tool to consider the inhibition of DNA damage repair was developed to model the combined effect of radiation and hyperthermia therapy. The outcomes suggested the further realization of radiobiological data for different types of tumors, temperatures, sequences, and oxygenation conditions, in addition to direct cell death and reoxygenation [112]. To improve patient selection and treatment plan optimization in thermoradiotherapy, a

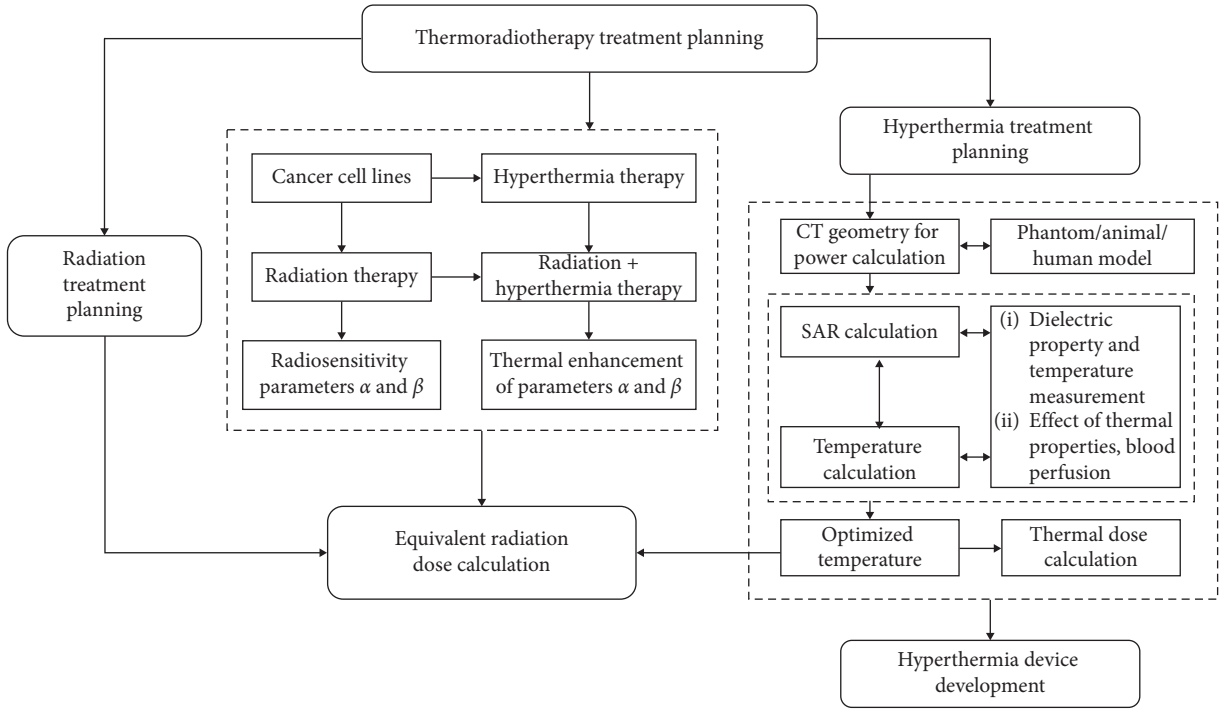

Figure 2: Thermoradiotherapy treatment planning for effective radiation treatment planning, HTP, equivalent radiation dose implementation, and hyperthermia treatment device development.

biological model as a function of variables was developed to predict treatment outcomes. The model describes cell survival dependency on dose, temperature, and time interval [113]. The effect of the time interval between radiotherapy and hyperthermia was evaluated to determine the therapeutic advantage of using biological modeling. The study demonstrated that the highest therapeutic gain for patients with cervical cancer was obtained in thermoradiotherapy when hyperthermia was immediately applied prior to or following radiation treatment [114].

7. Future Perspectives

For the effective clinical application of HTP, temperature-dependent blood perfusion and the dielectric properties of tumor tissues that consider variations according to patients and tumor stages require further investigations for various types of cancer. This may be investigated with the development of techniques, such as magnetic resonance electrical properties tomography (MREPT) and dictionary-based electric properties tomography (dbEPT) for measuring dielectric properties [115, 116] and high-frequency Doppler ultrasound and indocyanine green imaging for measuring blood perfusion [117, 118]. Although discrete vasculature (DIVA) models can provide sophisticated 3D vessel networks [119, 120] and software to model incomplete discrete vessel for the DIVA model from CT or MR angiography is available [121, 122], further developments and validations may need to obtain precise patient-specific temperature distribution in the vessel structures. For effective thermoradiotherapy planning based on equivalent radiation dose escalation, the determination of radiosensatization by hyperthermia on different cancer cell lines is required to apply this approach to various types of cancer. It may result in a treatment planning platform for combined hyperthermia and radiotherapy with high tumor control probability. To achieve this, improvements and updates in the theoretical framework and software tools require further development and validation. The development of a thermoradiotherapy planning strategy by integrating multiple treatment modalities may be an efficient way to enhance radiation treatment planning, HTP, equivalent radiation dose, and effective device development for combined radiation and hyperthermia therapy (Figure 2).

8. Conclusions

Studies have demonstrated the importance of simulations in the development of effective HTP techniques for clinical use. Dielectric properties and variations in blood perfusion are important in calculating energy deposition and temperature distribution in target tissues. Based on the accurate numerical modeling for hyperthermia treatment, efficient hyperthermia devices can be developed and the limitations of existing systems can be improved. Tissue damage and thermal dose calculations can predict the hot spots induced in applying RF energy, ensuring the safety and visualization of the lesion volume prior to treatment. Biological modeling for the calculation of an equivalent radiation dose may be effective for the quantification of thermoradiotherapy planning for combined hyperthermia and radiotherapy in clinics. The appropriate modeling and simulation of thermoradiotherapy is likely to contribute to

the prediction of the efficacy and toxicity of cancer thermal therapy.

Conflicts of Interest

The authors declare that there are no conflicts of interest regarding the publication of this paper.

Acknowledgments

This research was supported by the National Research Foundation sponsored by the Ministry of Science, ICT and Future Planning (NRF-2016R1A2B4012095) and the Ministry of Education (NRF-2016R1D1A1A09917195), Republic of Korea.

References

[1] J. Overgaard, S. M. Bentzen, J. Overgaard et al., "Randomised trial of hyperthermia as adjuvant to radiotherapy for recurrent or metastatic malignant melanoma," *The Lancet*, vol. 345, no. 8949, pp. 540–543, 1995.

[2] V. E. Kouloulias, J. R. Kouvaris, K. S. Nikita et al., "Intraoperative hyperthermia in conjunction with multi-schedule chemotherapy (pre-, intra- and post-operative), by-pass surgery, and post-operative radiotherapy for the management of unresectable pancreatic adenocarcinoma," *International Journal of Hyperthermia*, vol. 18, no. 3, pp. 233–252, 2002.

[3] C. A. Grieco, C. J. Simon, W. W. Mayo-Smith, T. A. DiPetrillo, N. E. Ready, and D. E. Dupuy, "Percutaneous image-guided thermal ablation and radiation therapy: outcomes of combined treatment for 41 patients with inoperable stage I/II non-small-cell lung cancer," *Journal of Vascular and Interventional Radiology*, vol. 17, no. 7, pp. 1117–1124, 2006.

[4] J. Sgouros, "Chemotherapy plus percutaneous radiofrequency ablation in patients with inoperable colorectal liver metastases," *World Journal of Gastrointestinal Oncology*, vol. 3, no. 4, pp. 60–66, 2011.

[5] B. Prasad, Y. H. Ha, S. K. Lee, and J. K. Kim, "Patient-specific simulation for selective liver tumor treatment with non-invasive radiofrequency hyperthermia," *Journal of Mechanical Science and Technology*, vol. 30, no. 12, pp. 5837–5845, 2016.

[6] H. P. Kok, P. Wust, P. R. Stauffer, F. Bardati, G. C. van Rhoon, and J. Crezee, "Current state of the art of regional hyperthermia treatment planning: a review," *Radiation Oncology*, vol. 10, no. 1, p. 196, 2015.

[7] J. J. W. Lagendijk, "Hyperthermia treatment planning," *Physics in Medicine and Biology*, vol. 45, no. 5, pp. R61–R76, 2000.

[8] M. M. Paulides, P. R. Stauffer, E. Neufeld et al., "Simulation techniques in hyperthermia treatment planning," *International Journal of Hyperthermia*, vol. 29, no. 4, pp. 346–357, 2013.

[9] H. Kroeze, J. B. V. d. Kamer, A. A. C. D. Leeuw, and J. J. W. Lagendijk, "Regional hyperthermia applicator design using FDTD modelling," *Physics in Medicine and Biology*, vol. 46, no. 7, pp. 1919–1935, 2001.

[10] M. Franckena, R. Canters, F. Termorshuizen, J. van der Zee, and G. van Rhoon, "Clinical implementation of hyperthermia treatment planning guided steering: a cross over trial to assess its current contribution to treatment quality," *International Journal of Hyperthermia*, vol. 26, no. 2, pp. 145–157, 2010.

[11] Z. Rijnen, J. F. Bakker, R. A. M. Canters et al., "Clinical integration of software tool VEDO for adaptive and quantitative application of phased array hyperthermia in the head and neck," *International Journal of Hyperthermia*, vol. 29, no. 3, pp. 181–193, 2013.

[12] T. Juang, P. R. Stauffer, O. A. Craciunescu et al., "Thermal dosimetry characteristics of deep regional heating of non-muscle invasive bladder cancer," *International Journal of Hyperthermia*, vol. 30, no. 3, pp. 176–183, 2014.

[13] H. P. Kok, M. de Greef, P. P. Borsboom, A. Bel, and J. Crezee, "Improved power steering with double and triple ring waveguide systems: the impact of the operating frequency," *International Journal of Hyperthermia*, vol. 27, no. 3, pp. 224–239, 2011.

[14] G. Sreenivasa, J. Gellermann, B. Rau et al., "Clinical use of the hyperthermia treatment planning system HyperPlan to predict effectiveness and toxicity," *International Journal of Radiation Oncology∗Biology∗Physics*, vol. 55, no. 2, pp. 407–419, 2003.

[15] P. M. A. van Haaren, H. P. Kok, C. A. T. van den Berg et al., "On verification of hyperthermia treatment planning for cervical carcinoma patients," *International Journal of Hyperthermia*, vol. 23, no. 3, pp. 303–314, 2007.

[16] A. D. Tinniswood, C. M. Furse, and O. P. Gandhi, "Computations of SAR distributions for two anatomically based models of the human head using CAD files of commercial telephones and the parallelized FDTD code," *IEEE Transactions on Antennas and Propagation*, vol. 46, no. 6, pp. 829–833, 1998.

[17] H. Zhao, S. Crozier, and F. Liu, "Finite difference time domain (FDTD) method for modeling the effect of switched gradients on the human body in MRI," *Magnetic Resonance in Medicine*, vol. 48, no. 6, pp. 1037–1042, 2002.

[18] R. P. Findlay and P. J. Dimbylow, "Effects of posture on FDTD calculations of specific absorption rate in a voxel model of the human body," *Physics in Medicine and Biology*, vol. 50, no. 16, pp. 3825–3835, 2005.

[19] R. P. Findlay and P. J. Dimbylow, "FDTD calculations of specific energy absorption rate in a seated voxel model of the human body from 10 MHz to 3 GHz," *Physics in Medicine and Biology*, vol. 51, no. 9, pp. 2339–2352, 2006.

[20] P. J. Dimbylow, "FDTD calculations of the whole-body averaged SAR in an anatomically realistic voxel model of the human body from 1 MHz to 1 GHz," *Physics in Medicine and Biology*, vol. 42, no. 3, pp. 479–490, 1997.

[21] C. M. Furse and O. P. Gandhi, "Calculation of electric fields and currents induced in a millimeter-resolution human model at 60 Hz using the FDTD method," *Bioelectromagnetics*, vol. 19, no. 5, pp. 293–299, 1998.

[22] J. B. V. d. Kamer, J. J. W. Lagendijk, A. A. C. D. Leeuw, and H. Kroeze, "High-resolution SAR modelling for regional hyperthermia: testing quasistatic zooming at 10 MHz," *Physics in Medicine and Biology*, vol. 46, no. 1, pp. 183–196, 2001.

[23] E. Pickwell, B. E. Cole, A. J. Fitzgerald, M. Pepper, and V. P. Wallace, "In vivo study of human skin using pulsed terahertz radiation," *Physics in Medicine and Biology*, vol. 49, no. 9, pp. 1595–1607, 2004.

[24] F. Gustrau, A. Bahr, M. Rittweger, S. Goltz, and S. Eggert, "Simulation of induced current densities in the human body at industrial induction heating frequencies," *IEEE*

Transactions on Electromagnetic Compatibility, vol. 41, no. 4, pp. 480–486, 1999.

[25] D. Sullivan, "Three-dimensional computer simulation in deep regional hyperthermia using the finite-difference time-domain method," *IEEE Transactions on Microwave Theory and Techniques*, vol. 38, no. 2, pp. 204–211, 1990.

[26] H. P. Kok, A. N. T. J. Kotte, and J. Crezee, "Planning, optimisation and evaluation of hyperthermia treatments," *International Journal of Hyperthermia*, vol. 33, no. 6, pp. 593–607, 2017.

[27] H. P. Kok and J. Crezee, "A comparison of the heating characteristics of capacitive and radiative superficial hyperthermia," *International Journal of Hyperthermia*, vol. 33, no. 4, pp. 378–386, 2017.

[28] N. Tsuda, K. Kuroda, and Y. Suzuki, "An inverse method to optimize heating conditions in RF-capacitive hyperthermia," *IEEE Transactions on Biomedical Engineering*, vol. 43, no. 10, pp. 1029–1037, 1996.

[29] B. Prasad, S. Kim, W. Cho, S. Kim, and J. K. Kim, "Effect of tumor properties on energy absorption, temperature mapping, and thermal dose in 13.56-MHz radiofrequency hyperthermia," *Journal of Thermal Biology*, vol. 74, pp. 281–289, 2018.

[30] H. H. Pennes, "Analysis of tissue and arterial blood temperatures in the resting human forearm," *Journal of Applied Physiology*, vol. 1, no. 2, pp. 93–122, 1948.

[31] F. Dughiero and S. Corazza, "Numerical simulation of thermal disposition with induction heating used for oncological hyperthermic treatment," *Medical & Biological Engineering & Computing*, vol. 43, no. 1, pp. 40–46, 2005.

[32] R. B. Roemer and T. C. Cetas, "Applications of bioheat transfer simulations in hyperthermia," *Cancer Research*, vol. 44, no. 10, pp. 4788–4799, 1984.

[33] S. A. Sapareto and W. C. Dewey, "Thermal dose determination in cancer therapy," *International Journal of Radiation Oncology∗Biology∗Physics*, vol. 10, no. 6, pp. 787–800, 1984.

[34] C. M. van Leeuwen, J. Crezee, A. L. Oei et al., "3D radiobiological evaluation of combined radiotherapy and hyperthermia treatments," *International Journal of Hyperthermia*, vol. 33, no. 2, pp. 160–169, 2017.

[35] C. Rossmann and D. Haemmerich, "Review of temperature dependence of thermal properties, dielectric properties, and perfusion of biological tissues at hyperthermic and ablation temperatures," *Critical Reviews in Biomedical Engineering*, vol. 42, no. 6, pp. 467–492, 2014.

[36] C. Gabriel, S. Gabriel, and E. Corthout, "The dielectric properties of biological tissues: I. literature survey," *Physics in Medicine and Biology*, vol. 41, no. 11, pp. 2231–2249, 1996.

[37] S. Gabriel, R. W. Lau, and C. Gabriel, "The dielectric properties of biological tissues: II. measurements in the frequency range 10 Hz to 20 GHz," *Physics in Medicine and Biology*, vol. 41, no. 11, pp. 2251–2269, 1996.

[38] S. Gabriel, R. W. Lau, and C. Gabriel, "The dielectric properties of biological tissues: III. parametric models for the dielectric spectrum of tissues," *Physics in Medicine and Biology*, vol. 41, no. 11, pp. 2271–2293, 1996.

[39] W. T. Joines, Y. Zhang, C. Li, and R. L. Jirtle, "The measured electrical properties of normal and malignant human tissues from 50 to 900 MHz," *Medical Physics*, vol. 21, no. 4, pp. 547–550, 1994.

[40] P. A. Hasgall, F. Di Gennaro, C. Baumgartner et al., "IT'IS database for thermal and electromagnetic parameters of biological tissues. Version 4.0," 2018.

[41] M. Lazebnik, D. Popovic, L. McCartney et al., "A large-scale study of the ultrawideband microwave dielectric properties of normal, benign and malignant breast tissues obtained from cancer surgeries," *Physics in Medicine and Biology*, vol. 52, no. 20, pp. 6093–6115, 2007.

[42] K. R. Foster and J. L. Schepps, "Dielectric properties of tumor and normal tissues at radio through microwave frequencies," *Journal of Microwave Power*, vol. 16, no. 2, pp. 107–119, 1981.

[43] D.-S. Yoo, "The dielectric properties of cancerous tissues in a nude mouse xenograft model," *Bioelectromagnetics*, vol. 25, no. 7, pp. 492–497, 2004.

[44] M. Raoof, B. T. Cisneros, S. J. Corr, F. Palalon, S. A. Curley, and N. V. Koshkina, "Tumor selective hyperthermia induced by short-wave capacitively-coupled RF electric-fields," *PLoS One*, vol. 8, no. 7, Article ID e68506, 2013.

[45] A. Peyman, B. Kos, M. Djokić et al., "Variation in dielectric properties due to pathological changes in human liver," *Bioelectromagnetics*, vol. 36, no. 8, pp. 603–612, 2015.

[46] Z. Li, W. Wang, Z. Cai et al., "Variation in the dielectric properties of freshly excised colorectal cancerous tissues at different tumor stages," *Bioelectromagnetics*, vol. 38, no. 7, pp. 522–532, 2017.

[47] M. T. Hossain, B. Prasad, K. S. Park et al., "Simulation and experimental evaluation of selective heating characteristics of 13.56 MHz radiofrequency hyperthermia in phantom models," *International Journal of Precision Engineering and Manufacturing*, vol. 17, no. 2, pp. 253–256, 2016.

[48] K. S. Kim, D. Hernandez, and S. Y. Lee, "Time-multiplexed two-channel capacitive radiofrequency hyperthermia with nanoparticle mediation," *BioMedical Engineering OnLine*, vol. 14, no. 1, p. 95, 2015.

[49] L. A. B. Varon, H. R. B. Orlande, and G. E. Eliçabe, "Estimation of state variables in the hyperthermia therapy of cancer with heating imposed by radiofrequency electromagnetic waves," *International Journal of Thermal Sciences*, vol. 98, pp. 228–236, 2015.

[50] K. S. Kim and S. Y. Lee, "Nanoparticle-mediated radiofrequency capacitive hyperthermia: a phantom study with magnetic resonance thermometry," *International Journal of Hyperthermia*, vol. 31, no. 8, pp. 831–839, 2015.

[51] M. E. Kowalski and J.-M. Jin, "A temperature-based feedback control system for electromagnetic phased-array hyperthermia: theory and simulation," *Physics in Medicine and Biology*, vol. 48, no. 5, pp. 633–651, 2003.

[52] S. Oh, Y.-C. Ryu, G. Carluccio, C. T. Sica, and C. M. Collins, "Measurement of SAR-induced temperature increase in a phantom and in vivo with comparison to numerical simulation," *Magnetic Resonance in Medicine*, vol. 71, no. 5, pp. 1923–1931, 2014.

[53] H. P. Kok, P. M. A. Van Haaren, J. B. Van de Kamer, J. Wiersma, J. D. P. Van Dijk, and J. Crezee, "High-resolution temperature-based optimization for hyperthermia treatment planning," *Physics in Medicine and Biology*, vol. 50, no. 13, pp. 3127–3141, 2005.

[54] H. P. Kok, J. Crezee, N. A. P. Franken, L. J. A. Stalpers, G. W. Barendsen, and A. Bel, "Quantifying the combined effect of radiation therapy and hyperthermia in terms of equivalent dose distributions," *International Journal of Radiation Oncology∗Biology∗Physics*, vol. 88, no. 3, pp. 739–745, 2014.

[55] J. Crezee, C. M. van Leeuwen, A. L. Oei et al., "Biological modelling of the radiation dose escalation effect of regional hyperthermia in cervical cancer," *Radiation Oncology*, vol. 11, no. 1, p. 14, 2016.

[56] R. F. Verhaart, G. M. Verduijn, V. Fortunati et al., "Accurate 3D temperature dosimetry during hyperthermia therapy by combining invasive measurements and patient-specific simulations," *International Journal of Hyperthermia*, vol. 31, no. 6, pp. 686–692, 2015.

[57] M. M. Paulides, J. F. Bakker, E. Neufeld et al., "The HYPERcollar: a novel applicator for hyperthermia in the head and neck," *International Journal of Hyperthermia*, vol. 23, no. 7, pp. 567–576, 2007.

[58] T. Drizdal, M. M. Paulides, N. van Holthe, and G. C. van Rhoon, "Hyperthermia treatment planning guided applicator selection for sub-superficial head and neck tumors heating," *International Journal of Hyperthermia*, vol. 34, no. 6, pp. 704–713, 2018.

[59] A. J. Surowiec, S. S. Stuchly, J. R. Barr, and A. Swarup, "Dielectric properties of breast carcinoma and the surrounding tissues," *IEEE Transactions on Biomedical Engineering*, vol. 35, no. 4, pp. 257–263, 1988.

[60] A. P. O'Rourke, M. Lazebnik, J. M. Bertram et al., "Dielectric properties of human normal, malignant and cirrhotic liver tissue: in vivo and ex vivo measurements from 0.5 to 20 GHz using a precision open-ended coaxial probe," *Physics in Medicine and Biology*, vol. 52, no. 15, pp. 4707–4719, 2007.

[61] F. Fu, S. X. Xin, and W. Chen, "Temperature- and frequency-dependent dielectric properties of biological tissues within the temperature and frequency ranges typically used for magnetic resonance imaging-guided focused ultrasound surgery," *International Journal of Hyperthermia*, vol. 30, no. 1, pp. 56–65, 2014.

[62] Z. Ji and C. L. Brace, "Expanded modeling of temperature-dependent dielectric properties for microwave thermal ablation," *Physics in Medicine and Biology*, vol. 56, no. 16, pp. 5249–5264, 2011.

[63] H. Kato and T. Ishida, "Development of an agar phantom adaptable for simulation of various tissues in the range 5–40 MHz. (Hyperthermia treatment of cancer)," *Physics in Medicine and Biology*, vol. 32, no. 2, pp. 221–226, 1987.

[64] C.-K. Chou, G.-W. Chen, A. W. Guy, and K. H. Luk, "Formulas for preparing phantom muscle tissue at various radiofrequencies," *Bioelectromagnetics*, vol. 5, no. 4, pp. 435–441, 1984.

[65] N. N. Graedel, J. R. Polimeni, B. Guerin, B. Gagoski, and L. L. Wald, "An anatomically realistic temperature phantom for radiofrequency heating measurements," *Magnetic Resonance in Medicine*, vol. 73, no. 1, pp. 442–450, 2015.

[66] H. Kato, K. Yoshimura, M. Kuroda et al., "Development of a phantom compatible for MRI and hyperthermia using carrageenan gel–relationship between dielectric properties and NaCl concentration," *International Journal of Hyperthermia*, vol. 20, no. 5, pp. 529–538, 2009.

[67] J. B. Leonard, K. R. Foster, and T. W. Athley, "Thermal properties of tissue equivalent phantom materials," *IEEE Transactions on Biomedical Engineering*, vol. 31, no. 7, pp. 533–536, 1984.

[68] J. J. W. Lagendijk and P. Nilsson, "Hyperthermia dough: a fat and bone equivalent phantom to test microwave/radiofrequency hyperthermia heating systems," *Physics in Medicine and Biology*, vol. 30, no. 7, pp. 709–712, 1985.

[69] M. Mcdonald, S. Lochhead, R. Chopra, and M. J. Bronskill, "Multi-modality tissue-mimicking phantom for thermal therapy," *Physics in Medicine and Biology*, vol. 49, no. 13, pp. 2767–2778, 2004.

[70] S. Langeland, J. D'hooge, T. Claessens et al., "RF-based two-dimensional cardiac strain estimation: a validation study in a tissue-mimicking phantom," *IEEE Transactions on Ultrasonics, Ferroelectrics and Frequency Control*, vol. 51, no. 11, pp. 1537–1546, 2004.

[71] C. Gabriel, "Tissue equivalent material for hand phantoms," *Physics in Medicine and Biology*, vol. 52, no. 14, pp. 4205–4210, 2007.

[72] Z. Wang, I. Aarya, M. Gueorguieva et al., "Image-based 3D modeling and validation of radiofrequency interstitial tumor ablation using a tissue-mimicking breast phantom," *International Journal of Computer Assisted Radiology and Surgery*, vol. 7, no. 6, pp. 941–948, 2012.

[73] R. K. Chen and A. J. Shih, "Multi-modality gellan gum-based tissue-mimicking phantom with targeted mechanical, electrical, and thermal properties," *Physics in Medicine and Biology*, vol. 58, no. 16, pp. 5511–5525, 2013.

[74] A. Dabbagh, B. J. J. Abdullah, C. Ramasindarum, and N. H. Abu Kasim, "Tissue-mimicking gel phantoms for thermal therapy studies," *Ultrasonic Imaging*, vol. 36, no. 4, pp. 291–316, 2014.

[75] O. I. Craciunescu, T. V. Samulski, J. R. MacFall, and S. T. Clegg, "Perturbations in hyperthermia temperature distributions associated with counter-current flow: numerical simulations and empirical verification," *IEEE Transactions on Biomedical Engineering*, vol. 47, no. 4, pp. 435–443, 2000.

[76] C. A. T. Van den Berg, L. W. Bartels, A. A. C. De Leeuw, J. J. W. Lagendijk, and J. B. Van de Kamer, "Experimental validation of hyperthermia SAR treatment planning using MR B_{1+}imaging," *Physics in Medicine and Biology*, vol. 49, no. 22, pp. 5029–5042, 2004.

[77] L. Winter, C. Özerdem, W. Hoffmann et al., "Design and evaluation of a hybrid radiofrequency applicator for magnetic resonance imaging and RF induced hyperthermia: electromagnetic field simulations up to 14.0 Tesla and proof-of-concept at 7.0 Tesla," *PLoS One*, vol. 8, no. 4, Article ID e61661, 2013.

[78] D. W. Armitage, H. H. LeVeen, and R. Pethig, "Radiofrequency-induced hyperthermia: computer simulation of specific absorption rate distributions using realistic anatomical models," *Physics in Medicine and Biology*, vol. 28, no. 1, pp. 31–42, 1983.

[79] J. A. Deford, C. F. Babbs, U. H. Patel, N. E. Fearnot, J. A. Marchosky, and C. J. Moran, "Accuracy and precision of computer-simulated tissue temperatures in individual human intracranial tumours treated with interstitial hyperthermia," *International Journal of Hyperthermia*, vol. 6, no. 4, pp. 755–769, 1990.

[80] T. Uzuka, R. Tanaka, H. Takahashi, K. Kakinuma, J. Matsuda, and K. Kato, "Planning of hyperthermic treatment for malignant glioma using computer simulation," *International Journal of Hyperthermia*, vol. 17, no. 2, pp. 114–122, 2001.

[81] C. A. T. V. d. Berg, L. W. Bartels, B. v. d. Bergen et al., "The use of MR B_{+1} imaging for validation of FDTD electromagnetic simulations of human anatomies," *Physics in Medicine and Biology*, vol. 51, no. 19, pp. 4735–4746, 2006.

[82] T. Voigt, H. Homann, U. Katscher, and O. Doessel, "Patient-individual local SAR determination: in vivo measurements and numerical validation," *Magnetic Resonance in Medicine*, vol. 68, no. 4, pp. 1117–1126, 2012.

[83] F. Bardati, A. Borrani, A. Gerardino, and G. A. Lovisolo, "SAR Optimization in a phased array radiofrequency hyperthermia system," *IEEE Transactions on Biomedical Engineering*, vol. 42, no. 12, pp. 1201–1207, 1995.

[84] J. Y. Chen and O. P. Gandhi, "Numerical simulation of annular-phased arrays of dipoles for hyperthermia of deep-seated tumors," *IEEE Transactions on Biomedical Engineering*, vol. 39, no. 3, pp. 209–216, 1992.

[85] J. Wiersma and J. D. P. Van Dijk, "RF hyperthermia array modelling; validation by means of measured EM-field distributions," *International Journal of Hyperthermia*, vol. 17, no. 1, pp. 63–81, 2001.

[86] P. Wust, M. Seebass, J. Nadobny, P. Deuflhard, G. Mönich, and R. Felix, "Simulation studies promote technological development of radiofrequency phased array hyperthermia," *International Journal of Hyperthermia*, vol. 25, no. 7, pp. 517–528, 2009.

[87] H. P. Kok, P. M. A. van Haaren, J. B. van de Kamer et al., "Prospective treatment planning to improve locoregional hyperthermia for oesophageal cancer," *International Journal of Hyperthermia*, vol. 22, no. 5, pp. 375–389, 2006.

[88] Z. Li, M. Vogel, P. F. MacCarini et al., "Improved hyperthermia treatment control using SAR/temperature simulation and PRFS magnetic resonance thermal imaging," *International Journal of Hyperthermia*, vol. 27, no. 1, pp. 86–99, 2011.

[89] M. M. Paulides, J. F. Bakker, A. P. M. Zwamborn, and G. C. van Rhoon, "A head and neck hyperthermia applicator: theoretical antenna array design," *International Journal of Hyperthermia*, vol. 23, no. 1, pp. 59–67, 2007.

[90] Z. Rijnen, P. Togni, R. Roskam, S. G. van de Geer, R. H. M. Goossens, and M. M. Paulides, "Quality and comfort in head and neck hyperthermia: a redesign according to clinical experience and simulation studies," *International Journal of Hyperthermia*, vol. 31, no. 8, pp. 823–830, 2015.

[91] G. M. Verduijn, E. M. de Wee, Z. Rijnen et al., "Deep hyperthermia with the HYPERcollar system combined with irradiation for advanced head and neck carcinoma—a feasibility study," *International Journal of Hyperthermia*, vol. 34, no. 7, pp. 994–1001, 2018.

[92] M. L. Van Der Gaag, M. De Bruijne, T. Samaras, J. Van Der Zee, and G. C. Van Rhoon, "Development of a guideline for the water bolus temperature in superficial hyperthermia," *International Journal of Hyperthermia*, vol. 22, no. 8, pp. 637–656, 2006.

[93] C.-C. Chen and J.-F. Kiang, "Electroquasistatic model of capacitive hyperthermia affected by heat convection," *Progress in Electromagnetics Research C*, vol. 89, pp. 61–74, 2019.

[94] P. Togni, Z. Rijnen, W. C. M. Numan et al., "Electromagnetic redesign of the HYPERcollar applicator: toward improved deep local head-and-neck hyperthermia," *Physics in Medicine and Biology*, vol. 58, no. 17, pp. 5997–6009, 2013.

[95] J. R. Oleson, T. V. Samulski, K. A. Leopold et al., "Sensitivity of hyperthermia trial outcomes to temperature and time: implications for thermal goals of treatment," *International Journal of Radiation Oncology∗Biology∗Physics*, vol. 25, no. 2, pp. 289–297, 1993.

[96] D. E. Thrall, G. L. Rosner, C. Azuma et al., "Using units of CEM 43°C T_{90}, local hyperthermia thermal dose can be delivered as prescribed," *International Journal of Hyperthermia*, vol. 16, no. 5, pp. 415–428, 2000.

[97] M. W. Dewhirst, B. L. Viglianti, M. Lora-Michiels, M. Hanson, and P. J. Hoopes, "Basic principles of thermal dosimetry and thermal thresholds for tissue damage from hyperthermia," *International Journal of Hyperthermia*, vol. 19, no. 3, pp. 267–294, 2003.

[98] E. L. Jones, J. R. Oleson, L. R. Prosnitz et al., "Randomized trial of hyperthermia and radiation for superficial tumors," *Journal of Clinical Oncology*, vol. 23, no. 13, pp. 3079–3085, 2005.

[99] D. E. Thrall, S. M. LaRue, D. Yu et al., "Thermal dose is related to duration of local control in canine sarcomas treated with thermoradiotherapy," *Clinical Cancer Research*, vol. 11, no. 14, pp. 5206–5214, 2005.

[100] M. de Bruijne, B. van der Holt, G. C. van Rhoon, and J. van der Zee, "Evaluation of CEM_{43}·CT_{90} thermal dose in superficial hyperthermia," *Strahlentherapie und Onkologie*, vol. 186, no. 8, pp. 436–443, 2010.

[101] G. Bruggmoser, S. Bauchowitz, R. Canters et al., "Quality assurance for clinical studies in regional deep hyperthermia," *Strahlentherapie und Onkologie*, vol. 187, no. 10, pp. 605–610, 2011.

[102] P. S. Yarmolenko, E. J. Moon, C. Landon et al., "Thresholds for thermal damage to normal tissues: an update," *International Journal of Hyperthermia*, vol. 27, no. 4, pp. 320–343, 2011.

[103] G. C. van Rhoon, T. Samaras, P. S. Yarmolenko, M. W. Dewhirst, E. Neufeld, and N. Kuster, "CEM_{43}°C thermal dose thresholds: a potential guide for magnetic resonance radiofrequency exposure levels?," *European Radiology*, vol. 23, no. 8, pp. 2215–2227, 2013.

[104] T.-C. Shih, H.-S. Kou, C.-T. Liauh, and W.-L. Lin, "The impact of thermal wave characteristics on thermal dose distribution during thermal therapy: a numerical study," *Medical Physics*, vol. 32, no. 9, pp. 3029–3036, 2005.

[105] M. Murbach, E. Neufeld, M. Capstick et al., "Thermal tissue damage model analyzed for different whole-body SAR and scan durations for standard MR body coils," *Magnetic Resonance in Medicine*, vol. 71, no. 1, pp. 421–431, 2014.

[106] F. Adibzadeh, M. M. Paulides, and G. C. van Rhoon, "SAR thresholds for electromagnetic exposure using functional thermal dose limits," *International Journal of Hyperthermia*, vol. 34, no. 8, pp. 1248–1254, 2018.

[107] J. C. Peeken, P. Vaupel, and S. E. Combs, "Integrating hyperthermia into modern radiation oncology: what evidence is necessary?," *Frontiers in Oncology*, vol. 7, p. 132, 2017.

[108] C. M. van Leeuwen, A. L. Oei, J. Crezee et al., "The alfa and beta of tumours : a review of parameters of the linear-quadratic model , derived from clinical radiotherapy studies," *Radiation Oncology*, vol. 13, no. 1, p. 96, 2018.

[109] F. Pajonk, A. van Ophoven, and W. H. McBride, "Hyperthermia-induced proteasome inhibition and loss of androgen receptor expression in human prostate cancer cells," *Cancer Research*, vol. 65, no. 11, pp. 4836–4843, 2005.

[110] N. A. P. Franken, A. L. Oei, H. P. Kok et al., "Cell survival and radiosensitisation: modulation of the linear and quadratic parameters of the LQ model," *International Journal of Oncology*, vol. 42, no. 5, pp. 1501–1515, 2013.

[111] B. Prasad, S. Kim, W. Cho et al., "Quantitative estimation of the equivalent radiation dose escalation using radiofrequency hyperthermia in mouse xenograft models of human lung cancer," *Scientific Reports*, vol. 9, no. 1, p. 3942, 2019.

[112] H. Crezee, C. M. van Leeuwen, A. L. Oei et al., "Thermoradiotherapy planning: integration in routine clinical practice," *International Journal of Hyperthermia*, vol. 32, no. 1, pp. 41–49, 2016.

[113] C. M. van Leeuwen, A. L. Oei, R. ten Cate et al., "Measurement and analysis of the impact of time-interval, temperature and radiation dose on tumour cell survival and its

application in thermoradiotherapy plan evaluation," *International Journal of Hyperthermia*, vol. 34, no. 1, pp. 30–38, 2018.

[114] C. M. van Leeuwen, J. Crezee, A. L. Oei et al., "The effect of time interval between radiotherapy and hyperthermia on planned equivalent radiation dose," *International Journal of Hyperthermia*, vol. 34, no. 7, pp. 901–909, 2018.

[115] X. Zhang, J. Liu, and B. He, "Magnetic-resonance-based electrical properties tomography : a review," *IEEE Reviews in Biomedical Engineering*, vol. 7, pp. 87–96, 2014.

[116] N. Hampe, M. Herrmann, T. Amthor, C. Findeklee, M. Doneva, and U. Katscher, "Dictionary-based electric properties tomography," *Magnetic Resonance in Medicine*, vol. 81, no. 1, pp. 342–349, 2019.

[117] D. E. Goertz, J. L. Yu, R. S. Kerbel, P. N. Burns, and F. S. Foster, "High-frequency Doppler ultrasound monitors the effects of antivascular therapy on tumor blood flow," *Cancer Research*, vol. 62, no. 22, pp. 6371–6375, 2002.

[118] F. Ishige, Y. Nabeya, I. Hoshino et al., "Quantitative assessment of the blood perfusion of the gastric conduit by indocyanine green imaging," *Journal of Surgical Research*, vol. 234, pp. 303–310, 2019.

[119] A. N. T. J. Kotte, G. M. J. van Leeuwen, and J. J. W. Lagendijk, "Modelling the thermal impact of a discrete vessel tree," *Physics in Medicine and Biology*, vol. 44, no. 1, pp. 57–74, 1999.

[120] A. Kotte, G. van Leeuwen, J. de Bree, J. van der Koijk, H. Crezee, and J. Lagendijk, "A description of discrete vessel segments in thermal modelling of tissues," *Physics in Medicine and Biology*, vol. 41, no. 5, pp. 865–884, 1996.

[121] G. M. J. van Leeuwen, A. N. T. J. Kotte, and J. J. W. Lagendijk, "A flexible algorithm for construction of 3-D vessel networks for use in thermal modeling," *IEEE Transactions on Biomedical Engineering*, vol. 45, no. 5, pp. 596–604, 1998.

[122] M. Prishvin, R. Zaridze, G. Bit-Babik, and A. Faraone, "Improved numerical modelling of heat transfer in human tissue exposed to RF energy," *Australasian Physical & Engineering Sciences in Medicine*, vol. 33, no. 4, pp. 307–317, 2010.